*Scientiae Radices*, **4**(2), 94-114 (2025)

Full Paper

SciRad SCIENTIAE RADICES

# Comparative Study of the Fluoride Ion Interaction with Small Fullerenes and POSS Cages

Mar Ríos-Gutiérrez(1), Bartłomiej Gostyński(2)✉

(1) Department of Organic Chemistry, University of Valencia,
Dr. Moliner 50, Burjassot, 46100 Valencia, Spain
(2) Centre of Molecular and Macromolecular Studies Polish Academy of Sciences
ul. Sienkiewicza 112 91-363 Łódź

✉ Correspondence to: bartlomiej.gostynski@cbmm.lodz.pl

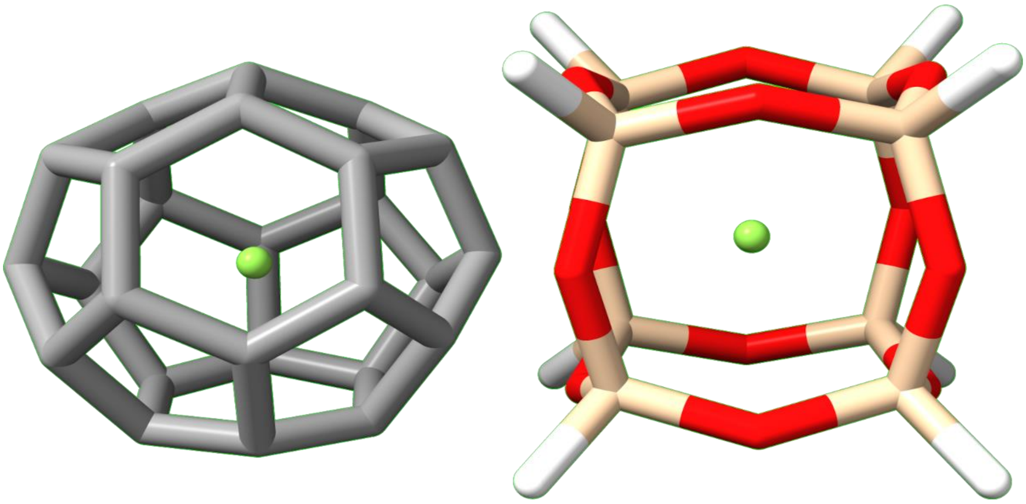

**Abstract:** This study investigates the encapsulation of the $F^-$ anion within fullerene and silsesquioxane (POSS) cage frameworks, using both Intermolecular Quantum Analysis (IQA) and Quantum Theory of Atoms in Molecules (QTAIM) at the DFT level of theory to analyze the effects of the $F^-$ presence on cage stability, as well as the nature of its interactions with the given framework. A detailed understanding of the energetic and electronic consequences of $F^-$ encapsulation is necessary to inform future design strategies for molecular encapsulation and ion stabilization in these and similar cage systems. The results suggest that the interaction between $F^-$ and the cage highly depends on steric and electronic factors; encapsulation generally destabilizes the cage, although certain systems show stabilization due to favorable interatomic interactions, as indicated by IQA analysis. The ion itself is stabilized in most systems, with POSS showing a significantly stronger stabilization than fullerenes. QTAIM analysis at bond critical points (BCPs) and cage critical points (CCPs) highlights the nature of the interactions, with electrostatic forces and charge redistribution being the primary stabilizing factors. The overall balance and stability of the $F^-$-cage complexes seem to be governed by the delicate interplay between steric compression and electrostatic interactions.

**Keywords:** DFT, IQA, QTAIM, Fluoride ion, Fullerenes, POSS, Interactions

**Received:** 2024.10.21
**Accepted:** 2025.05.28
**Published:** 2025.06.10
DOI: 10.58332/scirad2025v4i2a01

## Introduction

Fullerenes, characterized by their unique structure composed of carbon atoms arranged in a polyhedral cage, are widely recognized for their ability to host various molecules within their interior. This ability, referred to as encapsulation, provides a unique environment for studying interactions between encapsulated species and the hosting cage. Over the years, numerous studies have demonstrated the stability and unique chemical properties of fullerenes encapsulating small atoms [1], ions [2], and even small molecules [3,4].

Notably, fluoride ions ($F^-$), with their high electronegativity and small size, present an interesting case in the context of fullerene chemistry. Previous experimental work has shown that halide ions, such as $Cl^-$ and $Br^-$, can be encapsulated inside substituted, open fullerene cages.[2] The favourable interaction being largely driven by anion-π interactions, where the electron-deficient π-system of the carbon cage may interact with the encapsulated halogen anions. The encapsulation of ions ($F^-$ in particular) in fullerene cages is arguably able to significantly affect the electronic structure of the fullerene, as well as influence the reactivity of both the encapsulated species and the fullerene cage itself. In addition to fullerenes, another class of compounds has been shown to be able to encapsulate various species in a manner similar to them, including ions. These compounds, known as Polyhedral Oligomeric Silsesquioxanes (POSS) are organosilicon cage-like systems with structures based on silicon-oxygen linkages, usually substituted by organic groups in the cage corners.

The systems where entrapment of $F^-$ and other molecules with silsesquioxane cages took place with a closed cage has also been explored both experimentally by e.g. Bassindale et al. [5] and Bowers et al. [6] (see Fig. 1) and theoretically by Kudo [7]. These studies revealed that the fluoride $F^-$ ion can be encapsulated in the inner core of the cage, where it can interact with silicon Si atoms through coordination and electrostatic forces. The encapsulation is particularly relevant for the design of new materials, where the fluoride $F^-$ ion plays a pivotal role in catalyzing reactions, particularly in nucleophilic substitution processes [8]. This phenomenon is then of utmost importance in various fields, including materials science and nanotechnology.

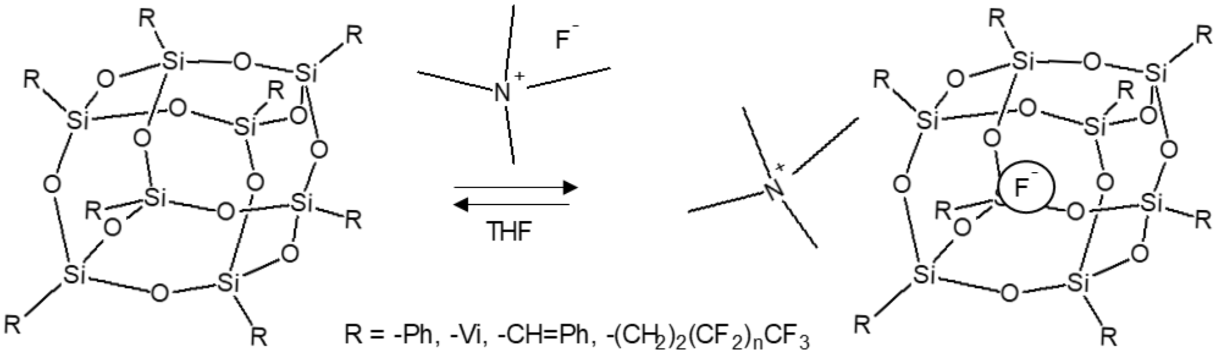

Fig. 1. Alkoxysilane condensation reaction forming a $T_8$-type silsesquioxane cage.

Interestingly, a literature search performed by us did not reveal any publications devoted specifically to the F- encapsulation by unsubstituted fullerenes whereas their functionalization by fluoride and other atoms remains a much more prevalent topic since several decades, see e.g. [9-11], especially for C60. Though one can stipulate that F-ion trapping could enhance bare fullerenes' properties in various areas, it might also introduce challenges such as potential unfavorable interactions, interference from other ions or environmental factors that could possibly affect the stability of such fullerene structures, especially small ones. This shows the need for more thoughtful and well-designed research in this area. Yet, there exist studies devoted to substituted $F^-$-encapsulated fullerenes as batteries, see e.g. [12] and references therein or to doped fullerenes as superconductors, albeit the doping is frequently done by use of metals, see e.g. [13]. All of this long-lasting research effort highlights the need for yet more studies on the properties and energetics of fullerenes, at the same time revealing rather the need for substitution and scaffold enrichment for these compounds.

This study aims to conduct a comparative investigation of the interactions between fluoride $F^-$ ion, silsesquioxane cages, and small fullerenes. The goal is to understand the nature of the interaction between the anion and the molecular cages and to determine how these interactions differ between fullerenes and silsesquioxanes. This study will consider various factors, including the structural characteristics of the cages, the electronegativity of the fluoride $F^-$ ion, and the nature of the interactions between $F^-$ and the molecular cage, using a theoretical approach. By comparing these interactions, we aim to gain insights that could potentially inform the design of novel materials for fluoride $F^-$ ion sensors and nano-sized reactors.

## Results and discussion

In the subsequent part, we discuss the research methodology as well as present the findings from both the Interacting Quantum Atoms (IQA) and Quantum Theory of Atoms in Molecules (QTAIM) analyses. The outcomes are then discussed in terms of the stability of the cage frameworks upon fluoride encapsulation and the nature of the interactions between the $F^-$ anion and the cages. The IQA analysis reveals how fluoride affects the electronic structure and stability of both cage types, providing insights into the energetic contributions from steric and electronic factors, whereas QTAIM analysis shows the specifics of fluoride-cage interactions, offering a detailed picture of the electrostatic and covalent-like forces at play. The results demonstrate the critical role of both local and global electronic effects in determining the stability of fluoride-cage complexes. These findings serve as a foundation for understanding fluoride encapsulation in these systems and may further inform the design of future molecular encapsulation strategies and possible applications of such systems.

### Methodology and theoretical essentials

DFT calculations were performed with the B3LYP functional [14,15] and the double-zeta 6-31+G(d) basis set,[16] using the Berny analytical gradient method for optimizations [17,18] within the GAUSSIAN16 suite of programs [19]. Grimme's D3 dispersion corrections with Becke-Johnson damping[20] were included. All the structures were confirmed to be PES minima by vibrational analysis, and the scaling factor was chosen to be 0.98. Additionally, single point energies were calculated in triple-zeta 6-311++G(d,p) basis set to refine (whenever possible) the values of thermochemical potentials by means of those energies and correction contributions obtained by vibrational analysis in the double-zeta basis set. Molecular geometries were visualized using the GaussView [21] and ChimeraX [22] programs.

The IQA analysis was performed with the AIMAll package [23] using the corresponding gas-phase B3LYP-D3/6-31+G(d) monodeterminantal wavefunctions. In an IQA-D3 analysis, the total energy considered is the sum of the intra- and inter-atomic IQA components plus inter-atomic dispersion obtained from the D3 program by Grimme,[24] given that D3 is an additive scheme.

The IQA scheme divides the total energy into two main energy contributions: [25] the intra-atomic energy, $E_{intra}^{A}$ , and the interatomic energy, $V_{inter}^{AB}$ . The interatomic energy is in turn divided into two additional terms: the interatomic electrostatic energy (typically referred to as "classical"), $V_{cl}^{AB}$ , and the interatomic exchange-correlation energy, $V_{xc}^{AB}$ , in such a way that $V_{inter}^{AB} = V_{cl}^{AB} + V_{xc}^{AB}$ . While $E_{intra}^{A}$ has been associated with steric effects,[26] $V_{cl}$ is related to electrostatic interactions,[27,28] and $V_{xc}$ quantifies covalency.[29]

A straightforward extension of IQA, called Interacting Quantum Fragments (IQF),[30] is used thanks to the additivity of topological atoms. IQF consists of grouping IQA energy terms of convenient fragments of the system to allow for a more chemically meaningful analysis of the interactions taking place between groups of atoms. In this study, we have chosen the two interacting $F^-$ and cage (fullerene or silsesquioxane) frameworks, i.e. X = $F^-$ or Cage. By default, we consider the sum of all atomic energies belonging to the considered fragment. Relative energies are analyzed by difference between the IQA energies of each of the two interacting frameworks (X) at the $F^-$-cage systems and the corresponding IQA energies computed at the ground state of the isolated species. Thus, $\Delta$E(cage) = E(cage in $F^-$-cage) – E($F^-$-free cage). In the case of fluoride, only the relative $\Delta E_{IQA}$ and $\Delta E_{intra}$ energies can be obtained since the isolated $F^-$ presents no interatomic interactions. $V_{inter}$($F^-$) quantifies, therefore, the interatomic interaction between the $F^-$ and cage frameworks. The relative total, intra- and interatomic IQA energies are a measure of how much the involved species are destabilized (positive relative energies) or stabilized (negative relative energies) when going from their GS to the $F^-$-cage systems.

The Bader's QTAIM analyses [31] were conducted using Multiwfn 3.7 software packages.[32] In QTAIM, a critical point (CP) is a point in space where the gradient of the electron density equals zero, meaning the electron density neither increases nor decreases in any direction. There are four types of critical points in QTAIM, classified based on their rank (r) and signature (s), which are determined by the eigenvalues of the Hessian matrix (a matrix of second derivatives of the electron density):

1. Nuclear Critical Point (NCP), (3, –3), a local maximum in all three directions of space, usually located at the position of an atomic nucleus. Identifies the position of atomic nuclei in the molecule;
2. Bond Critical Point (BCP), (3, –1), a saddle point with a maximum in two directions (perpendicular to the bond) and a minimum in one direction (along the bond axis). It appears between two bonded atoms, indicating the presence of a bond between them;
3. Ring Critical Point (RCP), (3, +1), a minimum in two directions (within the plane of a ring) and a maximum in one direction (perpendicular to the plane). They are found at the center of cyclic structures, indicating the presence of a ring structure in the electron density;
4. Cage Critical Point (CCP), (3, +3), a local minimum in all three directions of space. It occurs inside a cage-like structure, indicating the presence of a void or enclosed region in the electron density.

The evaluation of the sign of the Laplacian of the electron density in combination with other indicators at the BCPs, such as the electron density ($\rho_{cp}$), the Lagrangian kinetic energy ($G_{cp}$) and the local energy density ($H_{cp}$), can offer valuable insight into the types of bonds that they are signatures of. These are the topological indicators that characterize the atomic interactions.[33] The atomic interactions can be classified[34-36] as open-shell (shared) interactions ($\nabla^2\rho_{cp} < 0$, $H_{cp} \ll 0$ ), transit (intermediate) interactions ($\nabla^2\rho_{cp} > 0$, $H_{cp} < 0$) and closed-shell interactions ($\nabla^2\rho_{cp} > 0$, $H_{cp} > 0$). Open-shell interactions involve covalent and polar covalent bonds;[35,37] intermediate interactions are partially covalent interactions which include coordinate (dative) bonds, strong hydrogen bonds, metallic bonds, etc.;[34,37,38] and closed-shell interactions include ionic bonds and weak intermolecular interactions, such as weak and medium hydrogen bonds, van der Waals interactions, etc.[34,37] The value of electron density at BCP is also an important characteristic.[39,40] Covalent interactions exhibit $\rho_{cp} > 0.14$ a.u.,[34] partially covalent (intermediate) interactions are characterized by $0.04 < \rho_{cp} < 0.12$ a.u.[34,41] and closed-shell (electrostatic) interactions are characterized by $\rho_{cp} < 0.04$ a.u.[42] Espinosa[35] proposed a useful criterion to characterize interactions at the CPs using an analysis of the ratio of the potential and kinetic energy electron density $|V_{cp}|/G_{cp}$. If $|V_{cp}|/G_{cp} > 2$, then the interaction is covalent in nature; if$1 < |V_{cp}|/G_{cp} < 2$ , then the interaction is only partially covalent; and if $|V_{cp}|/G_{cp} < 1$, then the nature of the interaction is purely non-covalent.

## Geometry optimization

Geometries of the fluoride $F^-$ anion, small fullerenes (**C20**, **C24**, **C26**, see Fig.2 and Fig.3) taken from previously published results by Ewels et al.[43] as well as small POSS cages of various symmetries (**T6**, **T8**, **T10**, see Fig.4 and Fig.5) were (re)optimized *in vacuo*, both with encapsulated fluoride $F^-$ anion as well as without it (the former case is denoted with **-F** addition to the compounds' names). The **T8** cage was additionally considered in two distinct symmetries - **T8$_{Oh}$** (arguably the most common symmetry, henceforth called **T8**) and **T8$_{C2v}$**, see Fig.4. To speed up the calculations, only hydrogen-substituted POSS were considered.

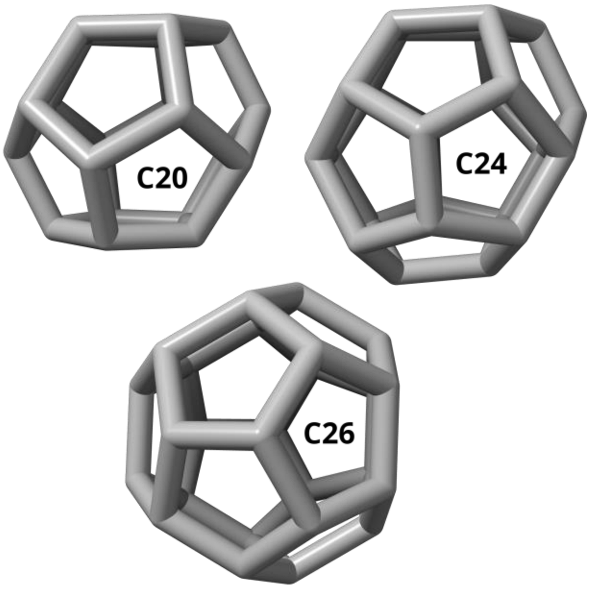

Fig. 2. Structures of the small fullerene cages considered without the F$^-$ anion.

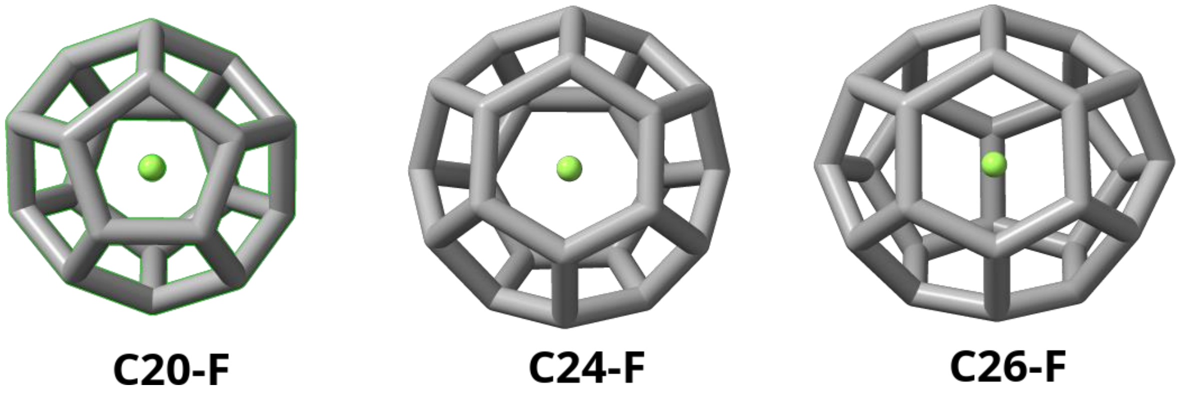

Fig. 3. Structures of the small fullerene cages considered with the F$^-$ anion.

## IQA analysis

In order to evaluate the effects of fluoride encapsulation on both the cage framework and the fluoride F$^-$ anion, an IQA analysis was performed. By examining the energy differences ($\Delta E$) of IQA energy terms for the cage and the F$^-$ anion, we aimed to determine the nature of the stabilization or destabilization induced by encapsulation.

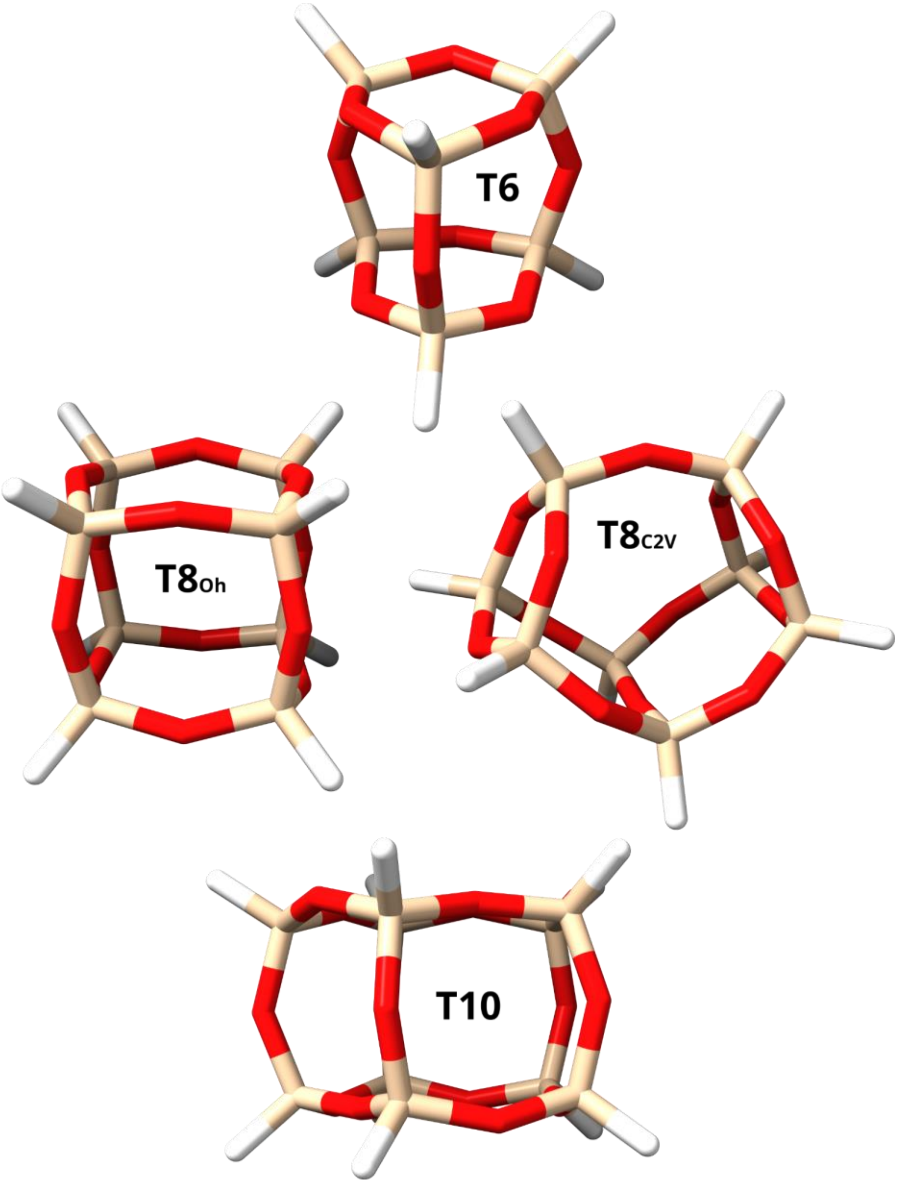

Fig. 4. Structures of the small POSS cages considered without the F$^-$ anion. The oxygen atoms of the Si-O-Si linkages are marked in red and substituting hydrogens in white.

### Impact of fluoride encapsulation on cage stability

Based on standard deviations, the energy of the cage is more affected than that of the fluoride F$^-$ anion upon encapsulation, suggesting that the cage undergoes greater electronic rearrangement than F$^-$ itself. In most cases, encapsulation destabilizes the cage, except in **T8-F** and **T10-F** where stabilization is observed ($\Delta E_{IQA}(cage)$ = −7.8 and −10.8 kcal·mol$^{-1}$, respectively).

A size-dependent trend is evident, where larger cages experience smaller perturbations upon fluoride inclusion. This is expected, as larger cages provide greater steric flexibility and electronic delocalization, allowing them to accommodate the anion with minimal structural strain.

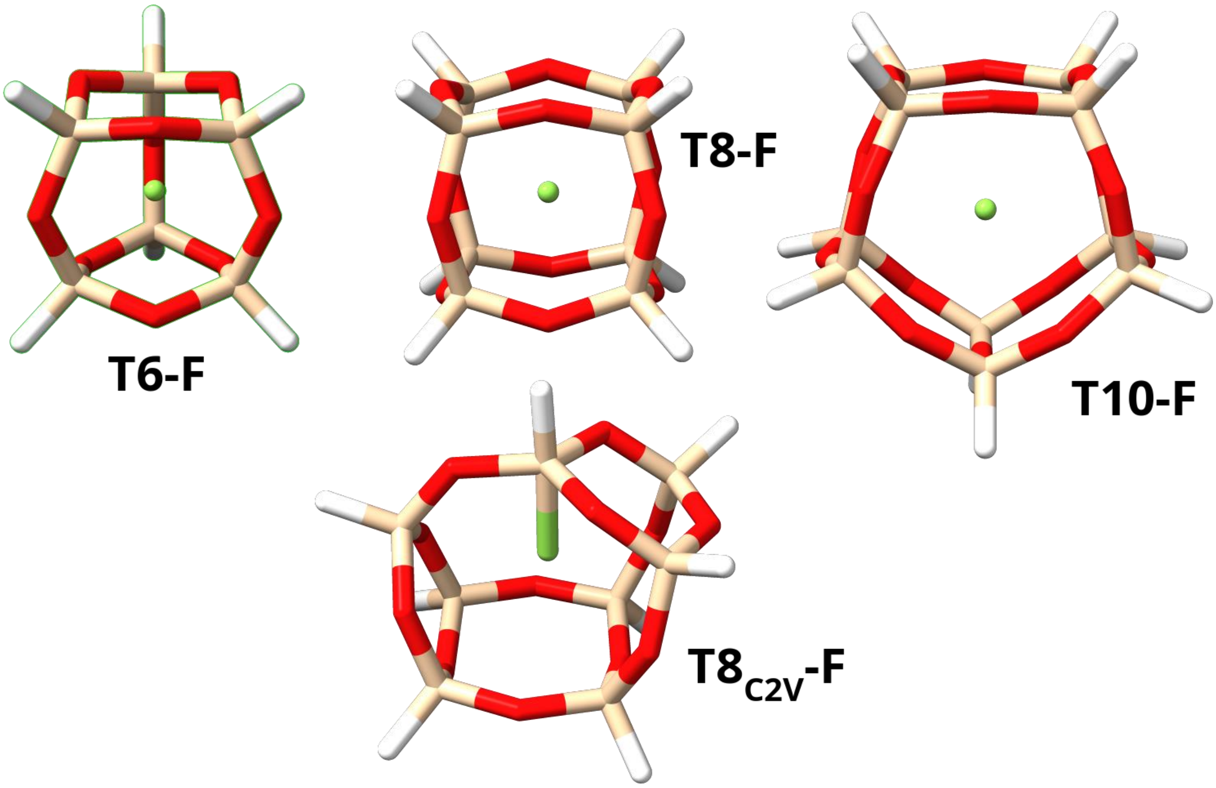

Fig. 4. Structures of the small POSS cages with the encapsulated F$^-$ anion. The oxygen atoms of the Si-O-Si linkages are marked in red and substituting hydrogens in white. A seeming Si-F bond is visible in the case of **T8$_{\mathrm{C2V}}$-F**.

The total energy difference ($\Delta E_{IQA}$) of the cage is determined by two main contributions: $\Delta E_{intra}$ (intra-atomic energy) and $\Delta V_{inter}$ (interatomic energy). Several key observations can be drawn from their relative magnitudes:

1. in most cases, both $\Delta E_{intra}(cage)$ and $\Delta V_{inter}(cage)$ are positive, supporting the general destabilization of the cages upon fluoride inclusion;
2. exceptions arise in specific systems: **T6-F** exhibits a negative $\Delta E_{intra}(cage)$ (–58.0 kcal·mol$^{-1}$), suggesting that steric hindrance within the cage is relieved upon encapsulation, leading to an unexpected structural stabilization. Likewise, $\Delta V_{inter}(cage)$ is negative in **T8-F**, **T8$_{\mathrm{C2V}}$-F**, and **T10-F**, indicating that in these systems, fluoride inclusion enhances intermolecular interactions within the cage, making the overall framework more stable;
3. in most systems, $\Delta V_{inter}(cage)$ dominates over $\Delta E_{intra}(cage)$, but this effect diminishes as cage size increases, being possible to be even reversed. For example, for **C26-F** and **T8$_{\mathrm{C2V}}$-F**, $\Delta E_{intra}(cage)$ exceeds $\Delta V_{inter}(cage)$, meaning that steric effects play a stronger role than intermolecular interactions in these cages;

4. the stabilization of **T8-F** and **T10-F** is primarily due to favorable interatomic interactions within the cage framework. These same stabilizing interactions are present in **T8C2v-F**, but due to the stronger unfavorable $\Delta E_{intra}(cage)$ contribution than $\Delta V_{inter}(cage)$, the net stabilization is neutralized;
5. overall, the relative balance between $\Delta E_{intra}(cage)$ and $\Delta V_{inter}(cage)$ determines whether the cage stabilizes or destabilizes upon fluoride encapsulation. The standard deviation of $\Delta V_{inter}(cage)$ terms shows that there is a more significant variation in the interatomic energy than in the intra-atomic one;
6. **T10-F** exhibits exceptionally large $\Delta E_{intra}(cage)$ and $\Delta V_{inter}(cage)$ values (>125 kcal·mol$^{-1}$ in absolute magnitude), surpassing all other systems where these values reach a maximum of ca. 83 kcal·mol$^{-1}$. This suggests a particularly strong electronic rearrangement in **T10-F** upon fluoride inclusion, possibly due to the redistribution of charge density within the cage.

Further decomposition of intermolecular interactions into exchange-correlation ($\Delta V_{xc}$) and classical electrostatic ($\Delta V_{cl}$) components reveals distinct trends between fullerene and silsesquioxane cages. While in fullerene cages, exchange-correlation (covalent-like effects) varies more significantly than electrostatics ($\Delta V_{xc}(cage) > \Delta V_{cl}(cage)$), in POSS cages, electrostatic stabilization is dominant ($\Delta V_{cl}(cage) > \Delta V_{xc}(cage)$). Interestingly, all $\Delta V_{xc}(cage)$ terms are positive, meaning that fluoride inclusion destabilizes the covalent-like interactions within the cage frameworks. Conversely, all $\Delta V_{cl}(cage)$ terms are negative, indicating that the redistribution of charge enhances electrostatic stabilization. A notable exception is **T6-F**, which is both covalently ($\Delta V_{xc}(cage)$) and electrostatically ($\Delta V_{cl}(cage)$) destabilized. These observations indicate that the overall stabilization of **T8-F** and **T10-F** is predominantly electrostatic in nature, rather than driven by quantum exchange-correlation effects.

Table 1. Difference between the IQA energy terms of the cage frameworks at the fluoride-containing and fluoride-free systems, in kcal·mol$^{-1}$.

| System | $\Delta E_{IQA}(cage)$ | $\Delta E_{intra}(cage)$ | $\Delta V_{inter}(cage)$ | $\Delta V_{xc}(cage)$ | $\Delta V_{cl}(cage)$ |
|---|---:|---:|---:|---:|---:|
| **C20-F** | 139.3 | 56.5 | 82.8 | 169.4 | −86.5 |
| **C24-F** | 102.8 | 50.0 | 52.9 | 102.1 | −49.2 |
| **C26-F** | 58.1 | 29.8 | 28.3 | 76.2 | −47.9 |
| **T6-F** | 13.9 | −58.0 | 71.9 | 1.6 | 70.3 |
| **T8-F** | −7.8 | 55.6 | −63.4 | 6.1 | −69.5 |
| **T8C2v-F** | 4.9 | 26.7 | −21.8 | 0.7 | −22.6 |
| **T10-F** | −10.8 | 129.7 | −140.5 | 18.0 | −158.5 |

Stabilization of fluoride in different cages

Unlike the cage, fluoride is significantly stabilized ($\Delta E_{IQA}(F^{-})$) in most systems by between 20.6 and 67.7 kcal·mol$^{-1}$, except in **C20-F**, where it is destabilized by 42.6 kcal·mol$^{-1}$. The strongest stabilization occurs in **T8$_{C2v}$-F** (−67.7 kcal·mol$^{-1}$), followed by **T8-F** (−63.6 kcal·mol$^{-1}$). In addition, fluoride stabilization in silsesquioxane cages is significantly stronger (ca. by 40 kcal·mol$^{-1}$) than in fullerene cages (**C24-F** and **C26-F**).

In order to investigate the origin of the F$^{-}$ stabilization, the two $\Delta E_{intra}(F^{-})$ and $V_{inter}(F^{-})$ terms were analyzed. $\Delta E_{intra}(F^{-})$ is always positive, reinforcing the idea that fluoride is sterically hindered upon encapsulation. This aligns with the "topological atom as a sponge" concept, where greater volume constraints lead to stronger intra-atomic repulsion.[44] Thus, smaller cage sizes impose greater compression of the fluoride atomic basin, increasing its internal destabilization. On the other hand, $V_{inter}(F^{-})$ is always negative, meaning that fluoride consistently forms favorable interactions with the cage framework. These $V_{inter}(F^{-})$ are ca. 20 and 60 kcal·mol$^{-1}$ stronger than $\Delta E_{intra}(F^{-})$ in the fullerenes and POSS systems, respectively, except **C20-F** in which the $\Delta E_{intra}(F^{-})$ dominates. This system **C20-F** is a remarkable case because, despite exhibiting the most favorable $V_{inter}(F^{-})$ (strongest interaction with the cage), it fails to stabilize fluoride due to its excessively unfavourable $\Delta E_{intra}(F^{-})$ contribution.

A notable finding is that fluoride-cage interactions ($V_{inter}(F^{-})$) in **C24-F** and **C26-F** are stronger than in the silsesquioxane cages **T8-F** and **T10-F** yet fluoride is better stabilized in the two latter systems. This highlights that overall fluoride stability ($\Delta E_{IQA}(F^{-})$) is not solely dictated by $V_{inter}(F^{-})$ but rather by the balance between electronic and steric effects. For instance, **T10-F**, despite having the least negative $V_{inter}(F^{-})$ (weakest stabilizing interaction), −92.3 kcal·mol$^{-1}$, is the second system where F$^{-}$ is the second system where F$^{-}$ is most stabilized overall due to its relatively low $\Delta E_{intra}(F^{-})$, 39.2 kcal·mol$^{-1}$, which minimizes steric repulsion and allows fluoride to remain stable; conversely, **C20-F**, which exhibits the strongest $V_{inter}(F^{-})$, −245.0 kcal·mol$^{-1}$ fails to stabilize fluoride effectively due to high $\Delta E_{intra}(F^{-})$ (287.6 kcal·mol$^{-1}$) which induces severe steric compression counteracting favorable interactions with the cage. Analysis of standard deviations reveals, indeed, that $\Delta E_{intra}(F^{-})$ exhibits the highest variation, confirming that steric effects, rather than electronic stabilization, primarily dictate fluoride stability.

Unlike the cage frameworks, both $V_{xc}(F^{-})$ and $V_{cl}(F^{-})$ are negative for fluoride, indicating that covalent-like and electrostatic interactions contribute favorably to its stabilization. In fullerenes, $V_{xc}(F^{-})$ dominates over $V_{cl}(F^{-})$, highlighting the primary role of exchange-correlation effects, while in POSS, electrostatics ($V_{cl}(F^-)$) play a stronger role, reinforcing that stabilization in these cages is primarily driven by charge distribution.

In summary, smaller cages exhibit stronger $V_{xc}(F^-)$ and $V_{cl}(F^-)$ interactions, but also experience greater steric repulsion ($\Delta E_{intra}(F^-)$), leading to a trade-off between interaction strength and steric constraints. Thus, while $V_{inter}(F^-)$ consistently favors fluoride stabilization, $\Delta E_{intra}(F^-)$ exhibits the highest variation, confirming that steric effects are the dominant factor in determining fluoride stability across different cages.

Table 2. Difference between the IQA energy terms of the fluoride anion at the fluoride-containing systems and the free fluoride anion, in kcal·mol$^{-1}$.

| System | $\Delta E_{IQA}(F^-)$ | $\Delta E_{intra}(F^-)$ | $V_{inter}(F^-)$ | $V_{xc}(F^-)$ | $V_{cl}(F^-)$ |
|---|---|---|---|---|---|
| **C20-F** | 42.6 | 287.6 | −245.0 | −164.7 | −80.4 |
| **C24-F** | −23.3 | 178.0 | −201.3 | −124.0 | −77.3 |
| **C26-F** | −20.6 | 154.3 | −174.9 | −121.0 | −53.9 |
| **T6-F** | −62.1 | 164.1 | −226.2 | −104.0 | −122.2 |
| **T8-F** | −63.6 | 81.9 | −145.5 | −65.5 | −80.0 |
| **T8$_{C2v}$-F** | −67.7 | 110.4 | −178.1 | −70.7 | −107.5 |
| **T10-F** | −53.1 | 39.2 | −92.3 | −38.2 | −54.2 |

## QTAIM analysis

The nature and strength of the interactions between the fluoride F$^-$ anion and the different fullerene and POSS cages were analyzed using QTAIM. The bond critical points (BCPs) connecting fluoride to the cage framework were identified, and the averages of key electronic parameters — including electron density ($\rho$), Laplacian of $\rho$ ($\nabla^2\rho$), kinetic energy density (G), potential energy density (V), total energy density (H), and the $|V|/G$ and $|G|/\rho$ ratios — were examined to classify and compare the interactions.

### Fluoride-Cage interactions at the BCPs

The electron density ($\rho$) at the BCPs provides an indication of bond strength, with higher values typically associated with stronger interactions. Among the studied systems, **C20-F** exhibits the highest electron density ($\rho$ = 0.0742 a.u.), suggesting a stronger interaction between F$^-$ and the cage, in agreement with the smaller size of this system. In contrast, **T10-F** has the lowest electron density ($\rho$ = 0.0086 a.u.), indicating a much weaker interaction, likely dominated by long-range electrostatic effects.

The Laplacian of electron density ($\nabla^2\rho$) is positive across all systems, indicating electrostatic or ionic interactions rather than strong covalent bonding. The highest values are observed in **C20-F** ($\nabla^2\rho$ = 0.3247 a.u.) and **C24-F** ($\nabla^2\rho$ = 0.1958 a.u.), which suggests that although these systems exhibit more electron density at the BCPs, the interactions remain electrostatic in nature. The lowest values are found in **T10-F** ($\nabla^2\rho$ = 0.0333 a.u.), indicating a weaker but still closed-shell interaction. This positive Laplacian trend is characteristic of ionic or van der Waals interactions, reinforcing the idea that the interaction between fluoride and the cage is not covalent but instead dominated by electrostatic attraction.

The potential energy density (V) and kinetic energy density (G) provide further insights into the nature of the F$^-$–cage interactions. The ratio $|V|/G$ is particularly useful in distinguishing covalent-like interactions ($|V|/G > 1$) from non-covalent or electrostatic interactions ($|V|/G < 1$). Systems **C20-F** ($|V|/G$ = 1.0881) and **T8$_{\text{C2v}}$-F** ($|V|/G$ = 1.2005) show the highest $|V|/G$ ratios, suggesting that these interactions have stronger electrostatic character with a more localized charge polarization. System **C24-F** ($|V|/G$ = 0.9921) is close to unity, indicating an almost entirely electrostatic interaction with little charge sharing. Finally, **T10-F** exhibits the lowest $|V|/G$ ratio (0.8535), consistent with a weak and predominantly non-covalent interaction.

The total energy density ($H = V + G$) provides further confirmation of the interaction strength. Systems with negative H (e.g. **C20-F**, **C26-F**, and **T6-F**) tend to exhibit stabilizing interactions, whereas systems with small or positive H values (e.g., **C24-F** and **T10-F**) suggest weaker, less stabilizing interactions between F$^-$ and the cage framework.

The $G/\rho$ ratio can be used as an indicator of bond strength and electron localization at the BCPs. Higher $G/\rho$ values (>1) suggest stronger, more localized interactions. Systems **C20-F** ($G/\rho$ = 1.2005) and **T8$_{\text{C2v}}$-F** ($G/\rho$ = 1.3225) exhibit the highest values, reinforcing their stronger electrostatic interactions with fluoride. On the other hand, **T6-F** and **T10-F** show lower $G/\rho$ values (< 0.85), indicative of weaker, more diffuse interactions.

These results suggest that fluoride is most strongly interacting in the **C20-F** and **T8$_{\text{C2v}}$-F** systems, where higher $\rho$ values and $|V|/G$ ratios exceeding unity indicate a stronger electrostatic interaction with the cage framework. **C26-F** also exhibits significant stabilization, but **T10-F** and **T8-F** show much weaker interactions, suggesting that fluoride is less stabilized within these cages and likely experiences weaker confinement. In any case, the interactions are fundamentally electrostatic in nature.

Table 3. Average values of the QTAIM parameters at the BCPs, in a.u.

| System | $\rho$ | $\nabla^2\rho$ | G | V | H | $\|V\|/G$ | $G/\rho$ |
|---|---|---|---|---|---|---|---|
| **C20-F** | 0.0742 | 0.3247 | 0.0890 | −0.0969 | −0.0078 | 1.0881 | 1.2005 |
| **C24-F** | 0.0424 | 0.1958 | 0.0486 | −0.0482 | 0.0004 | 0.9921 | 1.1465 |
| **C26-F** | 0.0424 | 0.1727 | 0.0440 | −0.0448 | −0.0008 | 1.0188 | 1.0378 |
| **T6-F** | 0.0340 | 0.0764 | 0.0290 | −0.0390 | −0.0099 | 1.3420 | 0.8535 |

| | | | | | | | |
|---|---|---|---|---|---|---|---|
| **T8-F** | 0.0172 | 0.0526 | 0.0140 | −0.0149 | −0.0009 | 1.0613 | 0.8140 |
| **T8$_{C2V}$-F** | 0.0415 | 0.1755 | 0.0549 | −0.0659 | −0.0110 | 1.2005 | 1.3225 |
| **T10-F** | 0.0086 | 0.0333 | 0.0073 | −0.0062 | 0.0011 | 0.8535 | 0.8435 |

Effect of fluoride encapsulation at the CCPs

To evaluate the impact of F$^-$ encapsulation on the electronic properties of the fullerene and POSS cages, we analyzed the differences in the averaged QTAIM parameters at the cage critical points (CCPs) between the F$^-$-containing and F$^-$-free systems. Only data for **C20**, **C26**, **T8$_{C2V}$-F** and **T10** were analyzed because for **C24-F**, **T6-F** and **T8-F** no CCPs could be found.

The electron density ($\Delta\rho$) at CCPs increases significantly upon fluoride encapsulation, with the highest changes observed for **C20** ($\Delta\rho$ = 0.0305 a.u.) and **C26** ($\Delta\rho$ = 0.0229 a.u.), while smaller but still noticeable increases occur for **T8$_{C2V}$-F** ($\Delta\rho$ = 0.0033 a.u.) and **T10** ($\Delta\rho$ = 0.0029 a.u.). This suggests that fluoride induces a global electron density redistribution within the cage, with larger effects in **C20** and **C26**, which may indicate a stronger stabilization or electron delocalization in these structures.

The Laplacian of electron density ($\Delta\nabla^2\rho$) follows a similar trend, indicating that F$^-$ promotes electron accumulation at the CCPs. Again, **C20** ($\Delta\nabla^2\rho$ = 0.2246 a.u.) and **C26** ($\Delta\nabla^2\rho$ = 0.1444 a.u.) exhibit the strongest effects, while **T8$_{C2V}$-F** ($\Delta\nabla^2\rho$ = 0.0183 a.u.) and **T10** ($\Delta\nabla^2\rho$ = 0.0151 a.u.) show more moderate changes.

The kinetic energy density ($\Delta G$) and potential energy density ($\Delta V$) at CCPs provide further insight into how fluoride influences the electronic stability of the cage. Both $\Delta G$ and $\Delta V$ are largest for **C20** ($\Delta G$ = 0.0491 a.u., $\Delta V$ = -0.0420 a.u.) and **C26** ($\Delta G$ = 0.0312 a.u., $\Delta V$ = −0.0263 a.u.), suggesting significant stabilization of the electron density within these cages upon fluoride encapsulation. In contrast, **T8$_{C2V}$-F** and **T10** exhibit smaller changes ($\Delta G$ = 0.0035 a.u., $\Delta V$ = −0.0024 a.u.), indicating weaker stabilization effects.

The total energy density ($\Delta H = \Delta V + \Delta G$) reflects the overall stabilization or destabilization induced by F$^-$ encapsulation. Systems **C20** ($\Delta H$ = 0.0071 a.u.) and **C26** ($\Delta H$ = 0.0049 a.u.) show slighter positive shifts, which may indicate enhanced electronic stability or redistribution of charge density.

As for the $|V|/G$ ratio, upon fluoride encapsulation, **C20** and **C26** exhibit a decrease in $|V|/G$ ($\Delta|V|/G$ = −0.1006 and −0.0447, respectively), suggesting a shift towards more electrostatic or delocalized interactions. Conversely, **T8$_{C2V}$-F** and **T10** exhibit an increase ($\Delta|V|/G$ = 0.1764 and 0.1027, respectively), suggesting that fluoride induces a slight increase in localized electronic effects within these cages. Regarding the $G/\rho$ ratio, **C20** exhibits the largest increase ($\Delta G/\rho$ = 0.5988), indicating that fluoride encapsulation significantly alters the electronic structure of this cage. Systems **T10** ($\Delta G/\rho$ = 0.4552) and **T8$_{C2V}$-F** ($\Delta G/\rho$ = 0.4845) show increases of similar magnitude to **C26** ($\Delta G/\rho$ = 0.4517), suggesting that fluoride has a comparable stabilizing effect on the electronic structure of these cages. All systems show positive $\Delta G/\rho$, suggesting that F$^-$ contributes to the overall electronic stabilization of the cage.

Table 4. Difference between the average values of the QTAIM parameters at the CCPs of the fluoride-containing and fluoride-free systems, in a.u.

| System | $\rho$ | $\nabla^2\rho$ | $\Delta G$ | $\Delta V$ | $\Delta H$ | $\Delta\lvert V\rvert/G$ | $\Delta G/\rho$ |
|---|---|---|---|---|---|---|---|
| **C20** | 0.0305 | 0.2246 | 0.0491 | −0.0420 | 0.0071 | −0.1006 | 0.5988 |
| **C26** | 0.0229 | 0.1444 | 0.0312 | −0.0263 | 0.0049 | −0.0447 | 0.4517 |
| **T8$_{C2V}$** | 0.0033 | 0.0183 | 0.0035 | −0.0024 | 0.0011 | 0.1764 | 0.4845 |
| **T10** | 0.0029 | 0.0151 | 0.0028 | −0.0018 | 0.0010 | 0.1027 | 0.4552 |

## Comparison between QTAIM analyses at CCPs and BCPs

The CCP Δ-data analysis provides information on global electron density redistribution within the cage upon fluoride encapsulation, while the BCP analysis focuses on the direct interactions between F$^-$ and the cage framework. By comparing trends between both analyses, we can assess whether F$^-$ stabilization at CCPs correlates with strong local F$^-$-cage interactions. Some appealing conclusions can be obtained:

1. strong F$^-$–cage interactions at BCPs correspond to larger CCP modifications: systems **C20** and **C26** exhibit the largest changes in CCP parameters ($\Delta\rho$, $\Delta\nabla^2\rho$, $\Delta V$, $\Delta G$, and $\Delta H$), suggesting that fluoride significantly alters the electronic structure of these cages upon encapsulation. These same systems also exhibit the highest electron density ($\rho$) at BCPs, confirming that strong local F$^-$–cage interactions (BCPs) correspond to significant global stabilization effects (CCPs). This correlation is due to increased electrostatic stabilization in certain cages;
2. weaker BCP interactions correspond to smaller CCP changes: systems **T8$_{C2V}$-F** and **T10** exhibit **lower Δ-values at CCP**, indicating that fluoride has a weaker effect on the electronic structure of these cages. Similarly, these systems also show lower electron density ($\rho$) at BCPs, suggesting weaker interactions with F$^-$. However, because the interactions at BCPs are fundamentally electrostatic (as indicated by the positive Laplacian values), the lower CCP perturbation in **T8$_{C2V}$-F** and **T10** suggests that the cages themselves provide weaker electrostatic stabilization for F$^-$, leading to reduced effects on the overall electron density distribution;
3. $\lvert V\rvert/G$ trends differ between BCPs and CCPs: at BCPs, $\lvert V\rvert/G$ is > 1 for most systems, suggesting moderate charge polarization rather than purely electrostatic confinement.

However, at CCPs, $|V|/G$ decreases in **C20** and **C26**, suggesting that fluoride encapsulation results in a redistribution of charge density, leading to delocalized stabilization rather than purely localized effects. This shift in $|V|/G$ from BCPs to CCPs suggests that fluoride plays a dual role: a) it forms localized electrostatic interactions with certain atoms in the cage (as seen in BCPs), and b) it also modifies the global electronic structure of the cage (as seen in CCP perturbations), particularly in systems like **C20** and **C26**.

These findings establish a clear correlation between local (BCP) and global (CCP) electronic effects, supporting a mechanistic interpretation in which fluoride enhances cage stability through a combination of localized electrostatic interactions and overall charge redistribution within the cage framework.

## Thermochemical analysis

As can be observed from the data present in Tables 5.-6., the formation of encapsulated fullerenes is strongly endothermic (42 – 187 kcal·mol$^{-1}$), while that of encapsulated POSS cages is significantly exothermic (40 – 64 kcal·mol$^{-1}$), according to the Gibbs free energy of formation; entropies exert a very mild effect, being negative by only 27-41 cal·(mol·K)$^{-1}$. Somewhat surprisingly though, the change of the basis set to the triple-zeta set does not introduce a uniform ameliorating trend for all the energetic outcomes; moreover - the entropic contributions are given only for double-zeta set as being impossible to account for without performing a proper vibrational analysis in a given basis due to the non-negligible vibrational entropy terms. The loss of entropic degrees of freedom thanks to the atomic movement restrictions due to the ion encapsulation can be detected as the increased $\Delta G$ values compared to $\Delta H$.

Table 5. Thermodynamical potential values for the encapsulation reactions leading to the given product for the double-zeta basis set. All values given in kcal·mol$^{-1}$, except the entropy contributions given in cal·(mol·K)$^{-1}$.

| Obtained product | $\Delta E_{ZPE}$ | $\Delta E$ | $\Delta H$ | $\Delta G$ | $\Delta S$ |
|---|---|---|---|---|---|
| **C20-F** | 177.9 | 178.0 | 177.5 | 186.7 | -31.1 |
| **C24-F** | 75.6 | 75.9 | 75.3 | 83.5 | -27.5 |
| **C26-F** | 33.7 | 33.4 | 32.8 | 42.3 | -31.8 |
| **T6-F** | -49.1 | -49.5 | -50.1 | -40.4 | -32.5 |
| **T8-F** | -74.8 | -75.4 | -76.0 | -63.8 | -40.9 |
| **T8$_{C2v}$-F** | -66.0 | -66.5 | -67.1 | -55.9 | -37.5 |
| **T10-F** | -68.7 | -68.7 | -69.3 | -58.2 | -37.4 |

Table 6. Thermodynamical potential values for the encapsulation reactions leading to the given product for the triple-zeta basis set. All values given in kcal·mol$^{-1}$.

| Obtained product | $\Delta E_{ZPE}$ | $\Delta E$ | $\Delta H$ | $\Delta G$ |
|---|---|---|---|---|
| **C20-F** | 180.6 | 180.8 | 180.2 | 189.5 |
| **C24-F** | 76.8 | 77.2 | 76.6 | 84.8 |
| **C26-F** | 34.2 | 34.0 | 33.4 | 42.8 |
| **T6-F** | -47.6 | -48.0 | -48.6 | -38.9 |
| **T8-F** | -75.4 | -76.0 | -76.6 | -64.4 |
| **T8$_{C2V}$-F** | -65.1 | -65.6 | -66.2 | -55.0 |
| **T10-F** | -71.2 | -71.2 | -71.8 | -60.7 |

Based on the presented outcomes, one can conclude that fluoride-containing small systems of unsubstituted fullerenes are unstable upon encapsulation of the ion, whereas an opposite trend emerges for POSS cages, with $T_8$ cage being the best host for this ion. The silicone cages seem thus to exhibit much better affinity to fluoride ion and as such, they are thus far more promising systems when the F$^-$-affinity exploitation is considered.

## Conclusions

This study presents a combined IQA and QTAIM analysis of fluoride encapsulation in small fullerene and silsesquioxane (POSS) cages. Both methods offer complementary insights into how F$^-$ interacts with and affects the stability of different host frameworks.

IQA results reveal that fluoride inclusion often destabilizes the cages, except in specific cases like **T8-F** and **T10-F**, where favorable interatomic interactions lead to net stabilization. Fluoride itself is stabilized in all systems except **C20-F**, where steric repulsion dominates despite strong interaction energies. Importantly, variations in intra-atomic energy ($\Delta E_{intra}(F^-)$) were shown to play a decisive role in fluoride stability, more so than interatomic contributions ($V_{inter}(F^-)$).

Energy decomposition showed that fullerenes stabilize F$^-$ mainly through exchange-correlation (covalent-like) interactions ($V_{xc}(F^-)$), while POSS rely more on electrostatics ($V_{cl}(F^-)$). QTAIM analysis confirmed the electrostatic nature of F$^-$–cage interactions and revealed that strong local interactions (at BCPs) correspond to broader electronic redistribution within the cage (at CCPs).

Overall, fluoride stabilization results from a balance between steric confinement and electrostatic attraction. Fullerenes and POSS cages exhibit distinct interaction patterns, but both can effectively confine F$^-$ under favorable geometric and electronic conditions: electrostatics dominates fluoride–POSS interactions, while fullerenes exhibit more exchange-correlation effects, yet the stability is ultimately controlled by steric factors. The results allow for a conclusion that a proper balance of steric and electronic factors is the main aspect to take into account when designing a framework for procuring new host-guest systems with tailored stabilization properties, since ion binding affects both local and global electronic structure in such systems.

## Acknowledgements

We gratefully acknowledge Polish high-performance computing infrastructure PLGrid (HPC Center: ACK Cyfronet AGH) for providing computer facilities and support within computational grant no. PLG/2014/000488. This project was also developed within the framework of the Vice Rectorate for Research's in-house program of the University of Valencia, Special Actions call, no. 20250098.

## References

[1] Sure, R.; Tonner, R.; Schwerdtfeger, P. A Systematic Study of Rare Gas Atoms Encapsulated in Small Fullerenes Using Dispersion Corrected Density Functional Theory. *J. Comput. Chem.* **2015**, 36, 88–96. DOI: 10.1002/jcc.23787

[2] Sun, S.; Liu, Z.; Colombo, F.; Gao, R.; Yu, Y.; Qiu, Y.; Su, J.; Gan, L. Open-Cage Fullerene as Molecular Container for $F^-$, $Cl^-$, $Br^-$ and $I^-$. *Angew Chem. Int. Ed. Engl.* **2022**, 61, e202212090. DOI: 10.1002/anie.202212090

[3] Slanina, Z.; Uhlık, F.; Lu, X.; Akasaka, T.; Adamowicz, L. H2O·HF@C70: Encapsulation Energetics and Thermodynamics. *Inorganics* **2023**, 11, 123. DOI: 10.3390/inorganics11030123

[4] Zhao, Y.; Hu, Z.; Chuai, P.; Jin, H.; Yang, S.; Su, J.; Shi, Z. Capturing Metal Fluoride inside a Carbon Cage. *J. Am. Chem. Soc.* **2024**, 146, 17003–17008. DOI: 10.1021/jacs.4c07045

[5] Bassindale, A. R.; Pourny, M.; Taylor, P. G.; Hursthouse, M. B.; Light, M. E. Fluoride-Ion Encapsulation within a Silsesquioxane Cage. *Angew Chem. Int. Ed. Engl.* **2003**, 42, 3488–3490. DOI: 10.1002/anie.200351249

[6] Anderson, S. E.; Bodzin, D. J.; Haddad, T. S.; Boatz, J. A.; Mabry, J. M.; Mitchell, C.; Bowers, M. T. Structural Investigation of Encapsulated Fluoride in Polyhedral Oligomeric Silsesquioxane Cages Using Ion Mobility Mass Spectrometry and Molecular Mechanics. *Chem. Mater.* **2008**, 20, 4299–4309. DOI: 10.1021/cm800058z

[7] Kudo, T.; Akasaka, M.; Gordon, M. S. Ab Initio Molecular Orbital Study of the Insertion of $H_2$ into POSS Compounds. *Theor. Chem. Acc.* **2008**, 120, 155–166. DOI:10.1007/s00214-007-0304-8

[8] Cypryk, M.; Gostynski, B.; Pokora, M. Hydrolysis of Trialkoxysilanes Catalysed by the Fluoride Anion. Nucleophilic vs. Basic Catalysis. *New J Chem.* **2019**, 43, 15222–15232. DOI: 10.1039/C9NJ03719E

[9] Selig, H.; Lifshitz, C.; Davidov, D.; Fischer, J.E. Fluorinated fullerenes: synthesis and characterization, *J. Fluor. Chem.* **1992**, 58, 256. DOI: 10.1016/S0022-1139(00)8079-5

[10] Boltalina, O. V.; Sidorov, L. N.; Bagryantsev, V. F.; Seredenko, V. A.; Zapol'skii, A. F.; Street, J. M.; Taylor, R. *J. Chem. Soc., Perkin Trans. 2* **1996**, 2275. DOI: 10.1039/P29960002275

[111] Boltalina, O. V. Fluorination of fullerenes and their derivatives, *J. Fluor. Chem.* **2000**, 101, 273.

[12] Hosseini, J.; Rastgou, A.; Moradi, R. F-encapsulated $B_{12}N_{12}$ fullerene as an anode for Li-ion batteries: A theoretical study, J*. Mol. Liq.* **2017**, 225, 913. DOI: 10.1016/j.molliq.2016.11.025

[13] Lieber, C. M.; Zhang, Z. Physical Properties of Metal-Doped Fullerene Superconductors, *Solid State Phys.* **1994***,* 48, 349 DOI: 10.1016/S0081-1947(08)60581-0

[14] Becke, A. D. Density-functional Thermochemistry. III. The Role of Exact Exchange. *J. Chem. Phys.* **1993**, 98, 5648–5652. DOI: 10.1063/1.464913

[15] Lee, C.; Yang, W.; Parr, R. G. Development of the Colle-Salvetti Correlation-Energy Formula into a Functional of the Electron Density. *Phys. Rev. B* **1988**, 37, 785–789. DOI: 10.1103/PhysRevB.37.785

[16] Hehre, W. J.; Radom, L.; Schleyer, P. v. R.; Pople, J. A. Ab Initio Molecular Orbital Theory. **1986**, Wiley: New York, NY.

[17] Schlegel, H. B. Optimization of Equilibrium Geometries and Transition Structures. *J. Comput. Chem.* **1982**, 3, 214–218. DOI: 10.1002/jcc.540030212

[18] Schlegel, H. B. Geometry Optimization On Potential Energy Surfaces, in.: Modern Electronic Structure Theory (Ed.: Yarkony, D. R.) World Scientific Publishing: Singapore, **1994**, 459–500. DOI: 10.1142/9789812832108_0008

[19] Frisch, M. J. et al. Gaussian16 Revision C.01. 2016; Gaussian Inc. Wallingford CT.

[20] Grimme, S.; Ehrlich, S.; Goerigk, L. Effect of the Damping Function in Dispersion Corrected Density Functional Theory. *J. Comput. Chem.* **2011**, 32, 1456–1465. DOI: 10.1002/jcc.21759

[21] Dennington, R.; Keith, T. A.; Millam, J. M. GaussView Version 6. 2019; Semichem Inc. Shawnee Mission KS.

[22] Pettersen, E. F.; Goddard, T. D.; Huang, C. C.; Meng, E. C.; Couch, G. S.; Croll, T. I.; Morris, J. H.; Ferrin, T. E. UCSF ChimeraX: Structure Visualization for Researchers, Educators, and Developers. *Prot. Sci.* **2021**, 30, 70–82. DOI: 10.1002/pro.3943

[23] AIMAll (Version 19.10.12), Todd A. Keith, TK Gristmill Software, Overland Park KS, USA, 2019 (aim.tkgristmill.com)

[24] Grimme, S.; Antony, J.; Ehrlich, S.; Krieg, H. A Consistent and Accurate Ab Initio Parametrization of Density Functional Dispersion Correction (DFT-D) for the 94 Elements H-Pu. *J. Chem. Phys.* **2010**, 132, 154104. DOI: 10.1063/1.3382344

[25] Blanco, M. A.; Pendas, A. M.; Francisco, E. Interacting Quantum Atoms: A Correlated Energy Decomposition Scheme Based on the Quantum Theory of Atoms in Molecules. *J. Chem. Theory Comput.* **2005**, 1, 1096–1109. DOI: 10.1021/ct0501093

[26] Wilson, A. L.; Popelier, P. L. A. Exponential Relationships Capturing Atomistic Short-Range Repulsion from the Interacting Quantum Atoms (IQA) Method. *J. Phys. Chem. A* **2016**, 120, 9647–9659. DOI: 10.1021/acs.jpca.6b10295

[27] Popelier, P. L. A.; Joubert, L.; Kosov, D. S. Convergence of the Electrostatic Interaction Based on Topological Atoms. *J. Phys. Chem. A* **2001**, 105, 8254–8261. DOI: 10.1021/jp011511q

[28] Popelier, P. L. A.; Kosov, D. S. Atom–Atom Partitioning of Intramolecular and Intermolecular Coulomb Energy. *J. Chem. Phys.* **2001**, 114, 6539–6547. DOI: 10.1063/1.1356013

[29] Pendas, A. M.; Francisco, E.; Blanco, M. A.; Gatti, C. Bond Paths as Privileged Exchange Channels. *Chem. Eur. J.* **2007**, 13, 9362–9371. DOI: 10.1002/chem.200700408

[30] Triestram, L.; Falcioni, F.; Popelier, P. L. A. Interacting Quantum Atoms and Multi-polar Electrostatic Study of XH· · ·π Interactions. *ACS Omega* **2023**, 8, 34844–34851. DOI: 10.1021/acsomega.3c04149

[31] Bader, R. F.; Tang, T. H.; Tal, Y.; Biegler-Koenig, F. W. Properties of atoms and bonds in hydrocarbon molecules. *J. Am. Chem. Soc.* **1982**, 104, 946–952. DOI: 10.1021/ja00368a004

[32] Lu, T.; Chen, F. Multiwfn: A Multifunctional Wavefunction Analyzer. *J. Comput. Chem.* **2012**, 33, 580–592. DOI: 10.1002/jcc.22885

[33] Bader, R. F. W. Atoms in Molecules: A Quantum Theory, 1st ed. **1994**, Clarendon Press: Oxford.

[34] Gatti, C. Chemical bonding in crystals: new directions. *Z. Kristallogr. Cryst. Mater.* **2005**, 220, 399–457. DOI: 10.1524/zkri.220.5.399.65073

[35] Espinosa, E.; Alkorta, I.; Elguero, J.; Molins, E. From Weak to Strong Interactions: A Comprehensive Analysis of the Topological and Energetic Properties of the Electron Density Distribution Involving X–H· · · F–Y Systems. *J. Chem. Phys.* **2002**, 117, 5529–5542. DOI: 10.1063/1.1501133

[36] Silvi, B. The Synaptic Order: A Key Concept to Understand Multicenter Bonding. *J. Mol. Struct.* **2002**, 614, 3–10. DOI: 10.1016/S0022-2860(02)00231-4

[37] Grabowski, S. J. What Is the Covalency of Hydrogen Bonding? *Chem. Rev.* **2011**, 111, 2597–2625. DOI: 10.1021/cr800346f

[38] Gervasio, G.; Bianchi, R.; Marabello, D. About the Topological Classification of the Metal–Metal Bond. *Chem. Phys. Lett.* **2004**, 387, 481–484. DOI: 10.1016/j.cplett.2004.02.043

[39] Popelier, P. L. A. The QTAIM Perspective of Chemical Bonding, in.: *The Chemical Bond*, (Ed.: Frenking, G.; Shaik, S.) Wiley, **2014**, 271–308. DOI:10.1002/9783527664696.ch8

[40] Bader, R. F. W. A Quantum Theory of Molecular Structure and Its Applications. *Chem. Rev.* **1991**, 91, 893–928. DOI: 10.1021/cr00005a013

[41] Ivanov, Y.; Nimura, T.; Tanaka, K. Electron Density and Electrostatic Potential of $KMnF_3$: A Phase-Transition Study. *Acta Crystallogr. B* **2004**, 60, 359–368. DOI: 10.1107/S0108768104009437

[42] Tsirelson, V.; Abramov, Y.; Zavodnik, V.; Stash, A.; Belokoneva, E.; Stahn, J.; Pietsch, U.; Feil, D. Critical Points in a Crystal and Procrystal. *Struct. Chem.* **1998**, 9, 249–254. DOI: 10.1023/A:1022474712532

[43] Tanuma, Y.; Maekawa, T.; Ewels, C. Methodological Investigation for Hydrogen Addition to Small Cage Carbon Fullerenes. *Cryst.* **2021**, 11, 1334. DOI: 10.3390/cryst11111334

[44] Popelier, P. L. A. On Quantum Chemical Topology, in.: *Applications of Topological Methods in Molecular Chemistry. Challenges and Advances in Computational Chemistry and Physics*, (Ed.: Chauvin, R., Lepetit, C., Silvi, B., Alikhani, E.) Wiley, **2016**, 23–52. DOI: 10.1007/978-3-319-29022-5_2